Cement and Concrete Research 38 (2008) 983–992

Contents lists available at ScienceDirect

Cement and Concrete Research

journal homepage: http://ees.elsevier.com/CEMCON/default.asp

# Hydration mechanisms of super sulphated slag cement

A. Gruskovnjak [a,*], B. Lothenbach [a], F. Winnefeld [a], R. Figi [a], S.-C. Ko [b], M. Adler [b], U. Mäder [c]

[a] Empa, Swiss Federal Laboratories for Materials Testing and Research, Laboratory for Concrete and Construction Chemistry, Ueberlandstrasse 129, CH-8600 Duebendorf, Switzerland
[b] Holcim Group Support Ltd., Product Innovation and Development, CH-5113 Holderbank, Switzerland
[c] University of Bern, Institute of Geological Sciences, Rock–Water-Interaction Group, CH-3012 Bern, Switzerland

ARTICLE INFO

*Article history:*
Received 25 October 2006
Accepted 4 March 2008

*Keywords:*
Granulated blast-furnace slag
Compressive strength
Acceleration
Hydration
Hydration products

ABSTRACT

The hydration and the strength evolution of supersulphated cements (SSC) produced by the activation of two different ground granulated blast furnace slags with anhydrite and small amounts of an alkaline activator have been investigated. The main differences between the two mixtures are found to be the strength development, the dissolution rate of the slags, the amount and volume of the individual hydration products formed and the growth mechanisms of the ettringite. The chemical composition of the slag had a large influence on the amount of the hydrates formed and thus on the volume of the hydrated slag.
Advancement of the amount of hydrates of a slag with low reactivity by adding aluminium sulphate and calcium hydroxide did increase the amount of ettringite. Nevertheless, the early compressive strength was not increased, but late strength shows a slow increase. It was concluded that the early compressive strength of an SSC using low reactive slag cannot be overcome by adding stoichiometric amounts of constituents which are used for the formation of a specific hydration product. The best way to increase early compressive strength is to increase the intrinsic dissolution rate.



## 1. Introduction

Slag cements are based on industrial by-products of the steel manufacture. This kind of cement helps to save natural raw materials and is thus decreasing the overall energy required to produce a cementitious material as well as reducing the carbon dioxide emissions.

Blast furnace slag (BFS) is the non-metallic by-product formed in a molten state simultaneously with iron in a blast furnace. The slag is derived from silicate and oxide components of the raw materials (iron ore, coke, lime or limestone) used in the smelting process. Little or no crystallisation occurs if the molten slag is cooled and solidified by rapid water quenching to a glassy state. This granular material is milled to a powder, the ground granulated blast furnace slag (GGBFS), which exhibits latent hydraulic properties.

The activation of GGBFS by sulphates was first described by Kühl in 1909 [1]. Generally, the super sulphated cements (SSC) consist of 80–85 wt.% of slag with 10–15 wt.% of anhydrite and an alkaline activator, often Portland cement clinker [2]. The main hydration products are ettringite and C–S–H [3,4]. SSC shows an increased resistance to sulphate attack and exhibits a lower heat of hydration compared to ordinary Portland cement (OPC). Slags, which are highly basic, react even in the sole presence of gypsum. Only slags with a low CaO-content need an additional activator (e.g., hydrated lime, clinker, alkali hydroxide) as an alkaline surrounding is necessary to achieve a sufficient reactivity.

The suitability of a slag for the use in cementitious materials depends primarily on its reactivity. The main factor which influences the reactivity of slag is the chemical and structural composition of the glass. Glasses with a high proportion of $Al_2O_3$ and CaO react faster and yield higher compressive strengths. Many attempts have been made to assess slags on the basis of moduli [5], which are based on bulk composition (oxide components). The simplest modulus and the most widely used to distinguish between "useful" and "non-useful" slag is $(CaO+MgO+Al_2O_3)/SiO_2$ [5]; but the effect of $Al_2O_3$ content is more complex [2] and cannot be fully described by this simple criterion.

In several studies slags with relatively high $Al_2O_3$-contents (11–28 wt.%) were activated with clinker and gypsum, anhydrite, lime or plaster of Paris [6–9] with or without additional activators [10,11]. Bijen and Niël [6] observed slower initial strength development with lower $Al_2O_3$ content (as low as 7 wt.%), but did not investigate the hydration mechanisms. No literature source was found which describes the hydration mechanisms of a SSC with a slag with $Al_2O_3$ content below 10 wt.%; here termed a slag with low reactivity (LR).

In this work the hydration mechanisms of a slag with low-reactivity (LR) is compared with that of a slag with a high reactivity (HR). Additionally, it was attempted to increase the low early (1 day) compressive strength of the LR-SSC through the promotion of

* Corresponding author. Tel.: +41 44 823 4718; fax: +41 44 823 4035.
*E-mail address:* astrid.gruskovnjak@empa.ch (A. Gruskovnjak).

0008-8846/$ – see front matter © 2008 Elsevier Ltd. All rights reserved.
doi:10.1016/j.cemconres.2008.03.004

**Table 1**
Chemical composition of HR- and LR-slag and the natural anhydrite used in wt.%

| Oxides | LR-SSC | HR-SSC | Natural anhydrite |
|---|---|---|---|
| | wt.% | wt.% | wt.% |
| LOI | 0.3 | −0.9 | 12.0 |
| $SiO_2$ | 37.9 | 34.1 | 3.6 |
| $Al_2O_3$ | 7.7 | 11.5 | 0.9 |
| $Fe_2O_3$ | 1.0 | 0.9 | 0.4 |
| CaO | 38.6 | 42.7 | 34.4 |
| MgO | 10.6 | 7.9 | 4.2 |
| $SO_3$ | 2.8 | 2.3 | 45.5 |
| $K_2O$ | 0.4 | 0.4 | 0.3 |
| $Na_2O$ | 0.2 | 0.2 | 0.1 |
| $TiO_2$ | 0.6 | 0.6 | 0.0 |
| $Mn_2O_3$ | 0.7 | 0.4 | 0.0 |
| $P_2O_5$ | 0.0 | 0.0 | 0.0 |
| Cl | 0.1 | 0.0 | n.a. |
| *Total* | 100.8 | 100.2 | 101.4 |

ettringite formation by adding an additional calcium, aluminium and sulphate source (LR_AC-SSC).

## 2. Materials and methods

The chemical composition of the samples was analyzed by X-ray fluorescence analysis (XRF) using a Philips PW 2400 instrument. The sulphide content in the slags was measured by iodometric titration of precipitated zinc sulphide according to the European Standard EN 196-2. The particle size distribution was determined with a laser granulometer Malvern Mastersizer X.

The experiments were carried out with two different slags, one with low reactivity (LR-slag) and one with high reactivity (HR-slag). The slag with the low reactivity (LR-slag) has a lower CaO and $Al_2O_3$, but a higher $SiO_2$ and MgO content compared to the HR-slag. Sulphur in the slag is originally present mainly as sulphide S(-II) (Table 1). X-ray diffraction (XRD) analysis (Fig. 1) shows that the HR-slag contains significant amounts of merwinite and some minor amounts of calcite and quartz; 85–90 wt.% of HR-slag is a silicate glass. LR-slag has a higher glass-content (≥97 wt.%). Some minor amounts of merwinite and calcite are present. The mineralogical composition was determined by XRD with a Panalytical X'Pert Pro powder diffractometer. The specific surface areas of the ground HR- and LR-slag are comparable (6'060 $cm^2/g$ and 5'520 $cm^2/g$, respectively). Ground HR-slag has a higher fraction of particles around 1 μm compared to LR-slag that shows a more bimodal distribution of particles with maxima near 2 μm and between 10–20 μm, respectively (Fig. 2).

To obtain SSC, both slags were activated with 15 wt.% natural anhydrite and 0.5 wt.% KOH. The natural anhydrite (cf. Table 1) used in SSC contains besides anhydrite significant amounts of gypsum (~24 wt.%), calcite (~12 wt.%) and dolomite (~3 wt.%) as determined by TGA analysis. TGA measurements were done under $N_2$-atmosphere at a heating rate of 20 K/min up to 1200 °C (Mettler Toledo TGA/SDTA851).

In a further step the composition of LR-SSC was modified with the addition of a mixture of 1 wt.% $Al_2(SO_4)_3{\cdot}16H_2O$ and 0.7 wt.% $Ca(OH)_2$ (stoichiometric amounts corresponding to ettringite). All pastes were prepared with a w/b ratio of 0.4 according to European Standard EN 196-3.

Mercury intrusion porosimetry (MIP) was measured on mortar samples with a water/binder ratio of 0.4. Compressive strength was determined according to European Standard EN 196-1 with a water/binder ratio adjusted to a constant flow of 200±20 mm according to EN 1015-3. Calorimetric measurements (Thermometric TAM Air) were carried out with 5 g of the fresh paste. The remaining material was filled in 0.5 l polyethylene bottles, sealed and stored under controlled conditions at 20 °C. Pore fluids of the hardened samples were extracted using the steel die method [12] with pressures up to 530 MPa. The solutions were filtered immediately (0.45 μm nylon filter). The pH was analyzed with a combined pH-electrode, which was calibrated using KOH solutions. The total concentrations of Al, Ca, Fe, K, Mg, Na and Si were determined by ICP-OES in samples diluted by a factor of 10 with dilute $HNO_3$ (1:9) to prevent the precipitation of solids. The concentrations of $SO_4^{2-}$, $SO_3^{2-}$ and $HS^-$ were determined by ion chromatography, iodometry and colorimetry [13]. A fraction of each solid paste was removed before pore fluid extraction, crushed and submersed in acetone to remove the pore solution. The samples were dried at 40 °C, ground to <63 μm and used for thermogravimetric (TGA) and X-ray diffraction (XRD) analysis. Samples were also examined by scanning electron microscopy (Philips ESEM FEG XL 30) using backscattered electron images (BSE) on polished samples and secondary electron images (SE) of freshly fractured samples.

Thermodynamic calculations were carried out using a consistent set of thermodynamic data [14,15] which had been originally compiled and verified for Portland cement systems [14–16]. A geochemical modelling program, GEMS [17], was used to calculate the concentration of the dissolved species as well as the kind and amount of solids precipitated. Based on the molar volume [$cm^3$/mol]

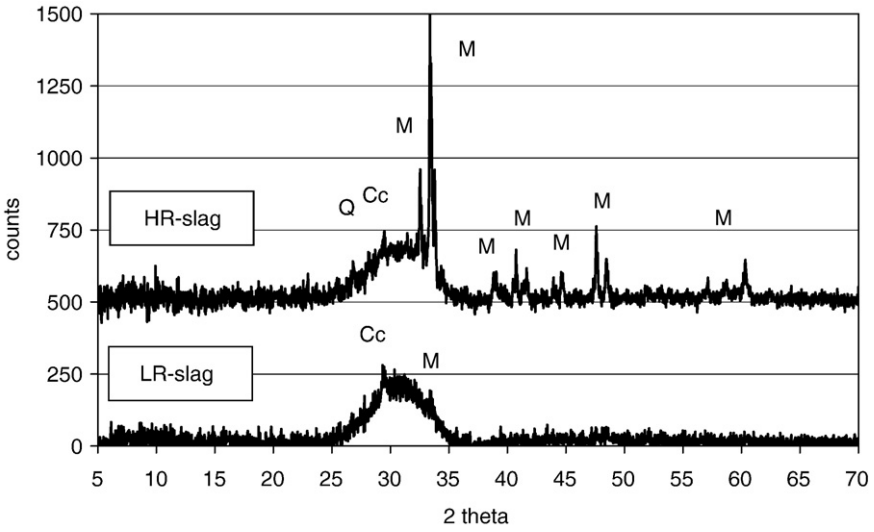


**Fig. 1.** XRD analyses of HR- and LR-slag in wt.%. M: merwinite, Cc: calcite, Q: quartz.

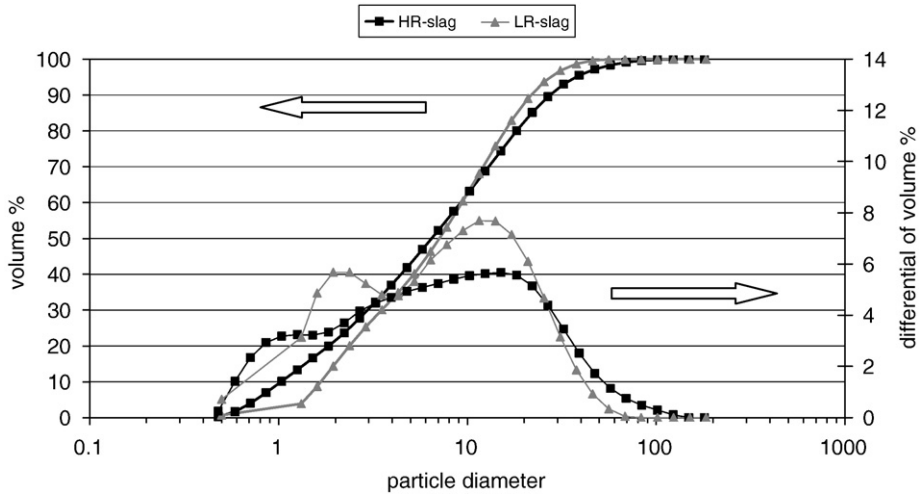


**Fig. 2.** Grain size distribution of LR- and HR-slag.

of the phases present in the sample [15], the volume of each individual hydrate as well as the total volume of the hydrating slag was calculated. The measured composition of the slag (XRF data, cf. Table 1) and the activators were used as input. For a detailed description of the setup it is referred to Lothenbach et al. [18]. For the sake of simplicity, it is assumed in the calculation that all anhydrite is transformed into gypsum, even though the XRD and TGA data show that this is a rather slow process. For the calculations it was considered that the slag dissolves uniformly and KOH, anhydrite and water equilibrate fast while the dissolution of the slag is very slow. Thus, the composition of the hydrate assemblage was calculated as a function of the fraction of slag dissolved assuming a thermodynamic equilibrium between the pore solution and the precipitating hydrates.

## 3. Results

### 3.1. Strength development, porosity and heat evolution

Both investigated SSCs, HR- and LR-SSC, show a similar 28-days strength (Table 2). However, the early strength development of the two systems shows significant differences. The SSC with the high-reactivity slag (HR-SSC) is characterized by a relatively high early strength (Table 2), but after two days, further strength development is slower than observed for LR-SSC.

It was attempted to increase the 1-day strength of LR-SSC by adding stoichiometric amounts (related to ettringite) of $Al_2(SO_4)_3{\cdot}16H_2O$ and $Ca(OH)_2$ to LR-SSC (LR_AC-SSC) with the intention to form additional ettringite. It was expected that the formation of additional ettringite during early hydration would decrease porosity and thus increase early compressive strength. Porosity measurements (Table 2) by MIP indicate in all cases a decrease in porosity with time.

**Table 2**
Compressive strength development (MPa) and total porosity (%) of HR-, LR- and LR-SSC with addition of $Al_2(SO_4)_3{\cdot}16H_2O$ and $Ca(OH)_2$ (LR_AC-SSC) after 1, 2, 7 and 28 days of hydration; total porosity was not measured after 2 days of hydration

| days of hydration | HR-SSC w/b=0.4 | LR-SSC w/b=0.4 | LR_AC-SSC w/b=0.4 |
|---|---|---|---|
| | MPa/% | MPa/% | MPa/% |
| 1 day | 10/19.4 | 3/19.0 | 0.7/18.8 |
| 2 days | 18/– | 7/– | 6/– |
| 7 days | 30/18.8 | 19/17.4 | 26/17.6 |
| 28 days | 38/18.4 | 32/16.2 | 45/16.3 |

A denser microstructure evolves as more hydrates are formed. The comparison of the strength and porosity data indicated large differences between the different slag systems. The determination of porosity by MIP may not be very representative of the total porosity due to inherent problems like the accessibility of pores and the influence of drying the specimen prior measurement [19].

Calorimetric measurements (Fig. 3) show that the heat flow evolution of the HR-SSC is characterized by a relatively short dormant period and an intense main hydration peak with a maximum at around 10 h. The LR-SSC system exhibits a relatively long dormant period, a very low heat flow and a wide main hydration peak with a maximum at 14 h. The low and retarded activity of LR-SSC is compatible with the observed slow strength development during the first day. LR_AC-SSC shows a higher heat flow evolution and a shorter dormant period in calorimetric analyses than LR-SSC (Fig. 3).

Strength development strongly depends on the kind and volume of the hydrates formed and thus on the interactions between solid and liquid components. The following sections are thus focused on these various aspects of hydration in order to explore the mechanisms behind the observed strength and heat flow developments in HR-, LR- and LR_AC-SSC.

### 3.2. Hydration products

Results of TGA analyses for HR-, LR- and LR_AC-SSC at different hydration times are given in Fig. 4. The comparison of the derivate curves in Fig. 4 with data for reference substances indicates the presence of ettringite, gypsum, AFm ($[Ca_2(Al,Fe)(OH)_6]{\cdot}X{\cdot}xH_2O$, where

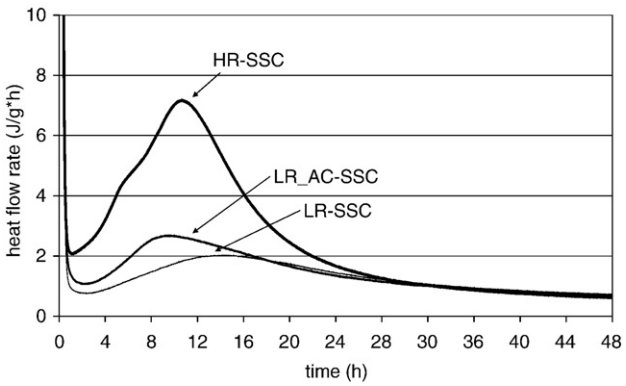


**Fig. 3.** Conduction calorimetry of HR-SSC and LR-SSC pastes, and of LR-SSC paste with addition of $Al_2(SO_4)_3{\cdot}16H_2O$ and $Ca(OH)_2$.

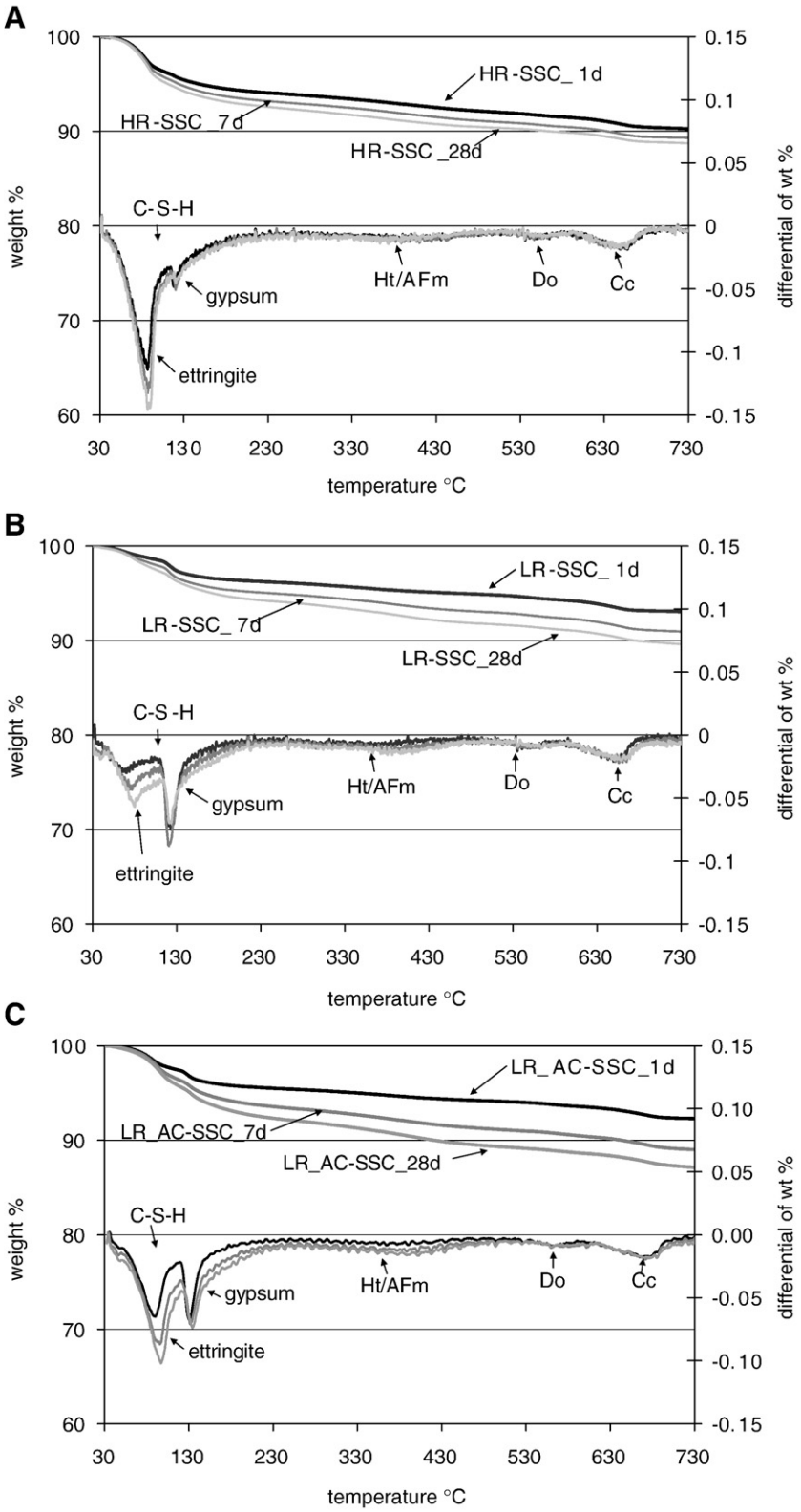


**Fig. 4.** TGA of A) HR-SSC, B) LR-SSC and C) LR-SSC with addition of $Al_2(SO_4)_3{\cdot}16H_2O$ and $Ca(OH)_2$ after 1, 7 and 28 days of hydration. Ht: hydrotalcite, Do: dolomite, Cc: calcite.

X denotes one formula unit of a single charged anion, or half a formula unit of a doubly charged anion) and/or (overlapping) hydrotalcite. Calcite and dolomite were already present in the raw material as minor phases; traces of calcite were present in the slag and calcite and dolomite in the natural anhydrite. Ettringite and gypsum are identified by XRD as well (Fig. 5). The C–S–H phase is not detectable by XRD, and in TGA it overlaps with ettringite and gypsum. Hydrotalcite overlaps with AFm phases in TGA analyses and with gypsum in XRD. In addition, anhydrite (from the activator added) and the main crystalline phase (merwinite) of the slag are observed in XRD

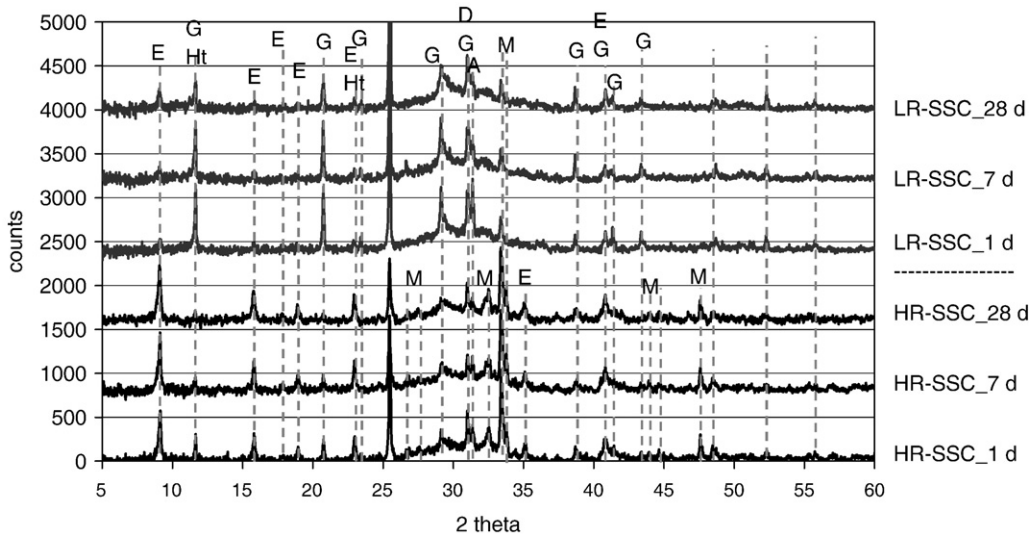


**Fig. 5.** XRD analyses of HR- SSC and LR-SSC after 1, 7 and 28 days of hydration. E: ettringite, G: gypsum, Ht: hydrotalcite, M: merwinite, A: anhydrite, D: dolomite.

analyses. The amount of merwinite, calcite, and dolomite (Figs. 4 and 5) is rather constant during the first 28 days. The amount of anhydrite decreases with time in both samples.

The total loss of weight of HR- and LR-SSC is similar after longer hydration times. After 1 day of hydration less water is bound in the hydration phases of LR-SSC, but after 7 and 28 days the value is comparable even though the amount of individual hydration phases is different. HR-SSC forms much more ettringite and less secondary gypsum than LR-SSC where secondary gypsum is the main hydration product followed by ettringite. LR_AC-SSC shows a higher total loss of weight compared to LR-SSC throughout all hydration times (Fig. 4) due to the additional ettringite formation promoted by the additives.

### 3.3. Pore solution chemistry

In both SSC systems (HR and LR), the composition of the pore solution is dominated by KOH (alkali activator) and sulphur in different oxidation states (Table 3): sulphate S(VI) from the dissolution of the natural anhydrite and sulphide S(-II) from the dissolution of slag. The sulphide and sulphate present transform partially to thiosulphate ($S_2O_3^{2-}$) and sulphite ($SO_3^{2-}$) [18,20–22]. The added KOH dissolves rapidly and leads to high concentrations of alkali hydroxide in solution and maintains a pH value of 12.6–13.0 (after 8h) in the pore solution which promotes the dissolution of the slag (Table 3).

The concentrations of elements analysed in the pore solution of HR- and LR-SSC were generally similar (Table 3, Fig. 6). The concentrations of Ca, Si, Al and $SO_3^{2-}$ were relatively constant between 8 h and 28 days. During hydration the concentration of $HS^-$ increases while pH and $SO_4^{2-}$ concentrations decrease (Fig. 6). The concentration of Na increases in both systems with hydration time. LR-SSC has a slightly lower pH compared to HR-SSC.

For LR_AC-SSC pore solution was not analysed.

### 3.4. Thermodynamic modelling

In both systems, the formation of significant amounts of C–S–H, ettringite, gypsum and hydrotalcite (Fig. 7) is predicted by thermodynamic calculations. The amount of these minerals increases as more slag is dissolved. At the same time the amount of pore solution decreases as water is incorporated into the hydration phases. Similar amounts of C–S–H are calculated to form in both systems as a function of the amount of slag dissolved with a calculated C/S ratio of approximately 1.

At the same degree of hydration approximately six times less ettringite (Fig. 7) is calculated to form in the LR-SSC system compared to the HR-SSC system. The much lower amount of ettringite is consistent with the observed data from TGA and XRD (Figs. 4 and 5). Thermodynamic calculations indicate a significantly lower consumption of gypsum (see Fig. 7) in the LR-SSC system. A higher amount of hydrotalcite is calculated to form in the LR-SSC mixture. In addition, small amounts of FeS (mackinawite) are calculated to precipitate.

### 3.5. Microstructure

Backscattered electron images of polished samples hydrated for 1, 7 and 28 days are shown in Fig. 8. In HR-SSC (Fig. 8 A, C, E) significant

**Table 3**
Concentrations in the pore solution in HR- and LR-SSC after 8 h, 1, 7 and 28 days of hydration (in mmol/l)

| | | Ca | Si | Al | $SO_4^{2-}$ | $SO_3^{2-}$ | $HS^-$ | K | Na | pH |
|---|---|---|---|---|---|---|---|---|---|---|
| | Age | mmol/l | mmol/l | mmol/l | mmol/l | mmol/l | mmol/l | mmol/l | mmol/l | |
| HR-SSC | 8 h | 15 | 0.21 | 0.007 | 156 | 11 | 22 | 358 | 35 | 13.0 |
| HR-SSC | 1 day | 15 | 0.25 | 0.007 | 125 | 12 | 87 | 307 | 52 | 12.3 |
| HR-SSC | 7 days | 17 | 0.21 | 0.011 | 177 | 14 | 87 | 486 | 70 | 12.3 |
| HR-SSC | 28 days | 15 | 0.14 | 0.011 | 125 | 14 | 87 | 358 | 70 | 12.2 |
| LR-SSC | 8 h | 15 | 0.25 | 0.019 | 125 | 16 | 22 | 281 | 25 | 12.6 |
| LR-SSC | 1 day | 15 | 0.21 | 0.019 | 135 | 19 | 69 | 332 | 34 | 12.3 |
| LR-SSC | 7 days | 17 | 0.11 | 0.015 | 95 | 19 | 87 | 307 | 43 | 12.1 |
| LR-SSC | 28 days | 27 | 0.04 | 0.004 | 40 | 11 | 109 | 207 | 61 | 11.7 |

The concentrations of Mg, Fe, Cr and P were under the detection limit of 1 mg/l.

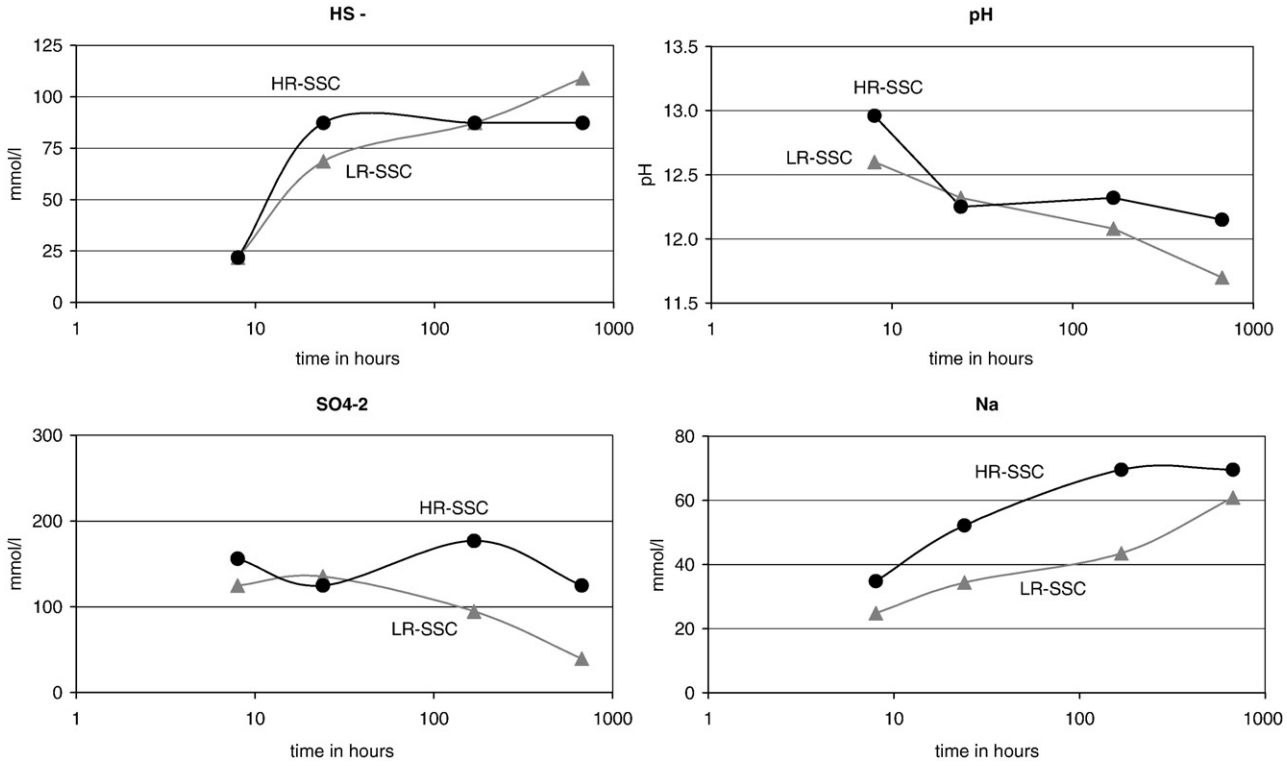


**Fig. 6.** Measured composition ($HS^-$, pH, $SO_4^{2-}$ and Na) of the pore solution of HR- and LR-SSC pastes after 8 h, 1, 7 and 28 days of hydration.

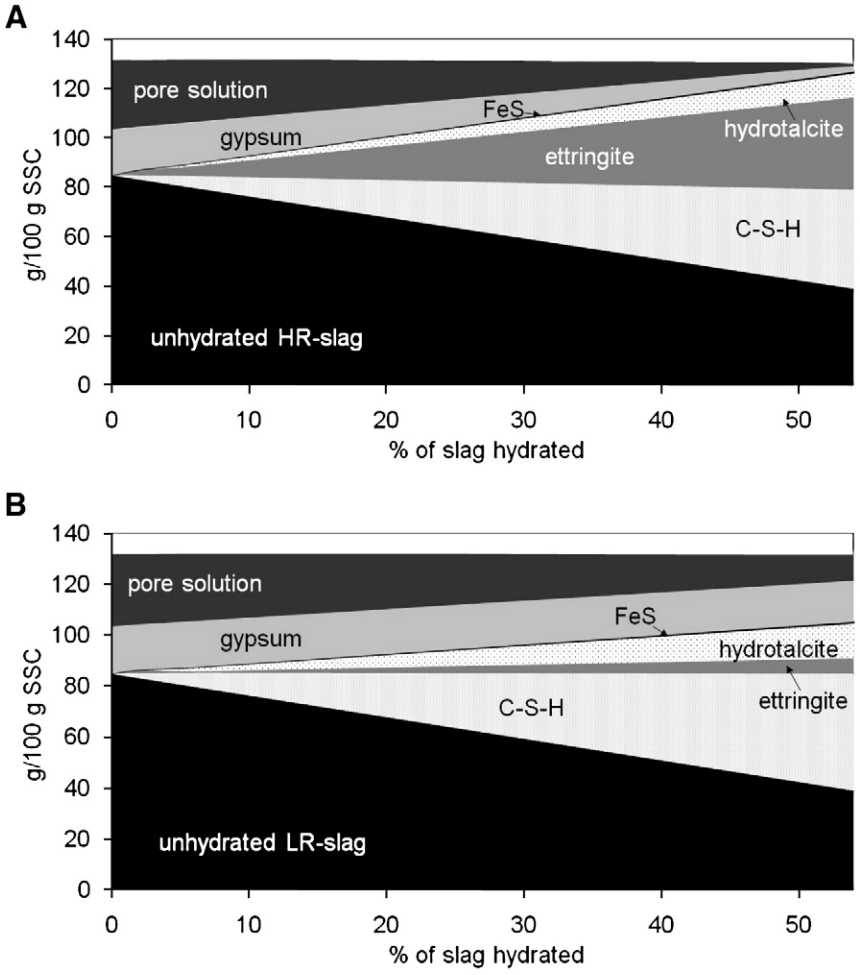


**Fig. 7.** Calculated composition of the phases present in A) HR-SSC B) LR-SSC as a function of slag dissolved.

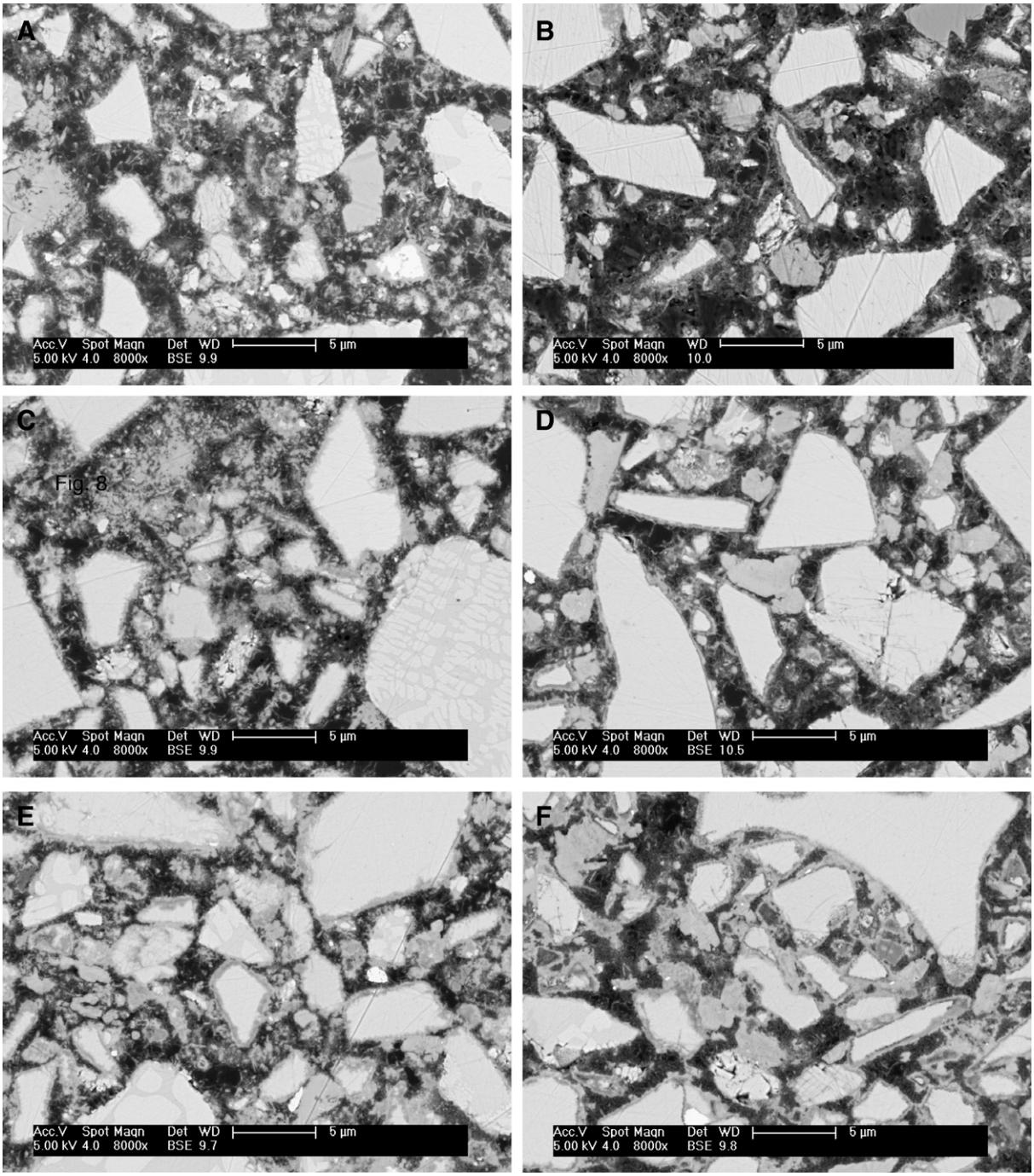


**Fig. 8.** Backscattered electron images of A, C, E) HR-SSC and B, D, F) LR-SSC after 1, 7 and 28 days of hydration.

quantities of hydration products have formed after 1 and 7 days. After 7 days small particles have hydrated mainly. Ettringite prisms can be observed reaching out from the slag particles into the pore space, giving the sample a bristle air. In LR-SSC (Fig. 8 B, D, F) much less hydrates are present after 1 and 7 days. After 7 days smaller particles show a hydration rim, but are not yet fully hydrated. Ettringite prisms as in HR-SSC cannot be observed. C–S–H fibres fill the pore space continuously.

ESEM investigations of fractured surfaces of HR-SSC (Fig. 9 A/B) show that the hydration products formed after 1 day cover the slag particles and are well interlocked. Ettringite forms long thin hexagonal prisms; after one day of hydration they have a length of ~1 μm. The prisms mainly grow perpendicular to the surface of the slag particles. The C–S–H phase is reticular. The two phases are closely intermixed in the matrix.

The slag particles in LR-SSC are covered and surrounded by only a thin hydration layer after 1 day of hydration (Fig. 9 C/D) with a significant fraction of pore space still present. The hydration layer forms a loose network of C–S–H phases. Some needles or prisms of ettringite crystals occur parallel to the surface of larger slag particles, but are mainly present as nests in the pore space (Fig. 9 D). The prisms have a length of around 1–1.5 μm. A large amount of secondary gypsum is observed, which is hardly ever surrounded by hydration phases.

In LR_AC-SSC (Fig. 9 E/F) a higher amount of smaller ettringite crystals is observed in the SE images than in LR-SSC. The ettringite forms nests in the pore space (Fig. 9 F) and grows individually on the

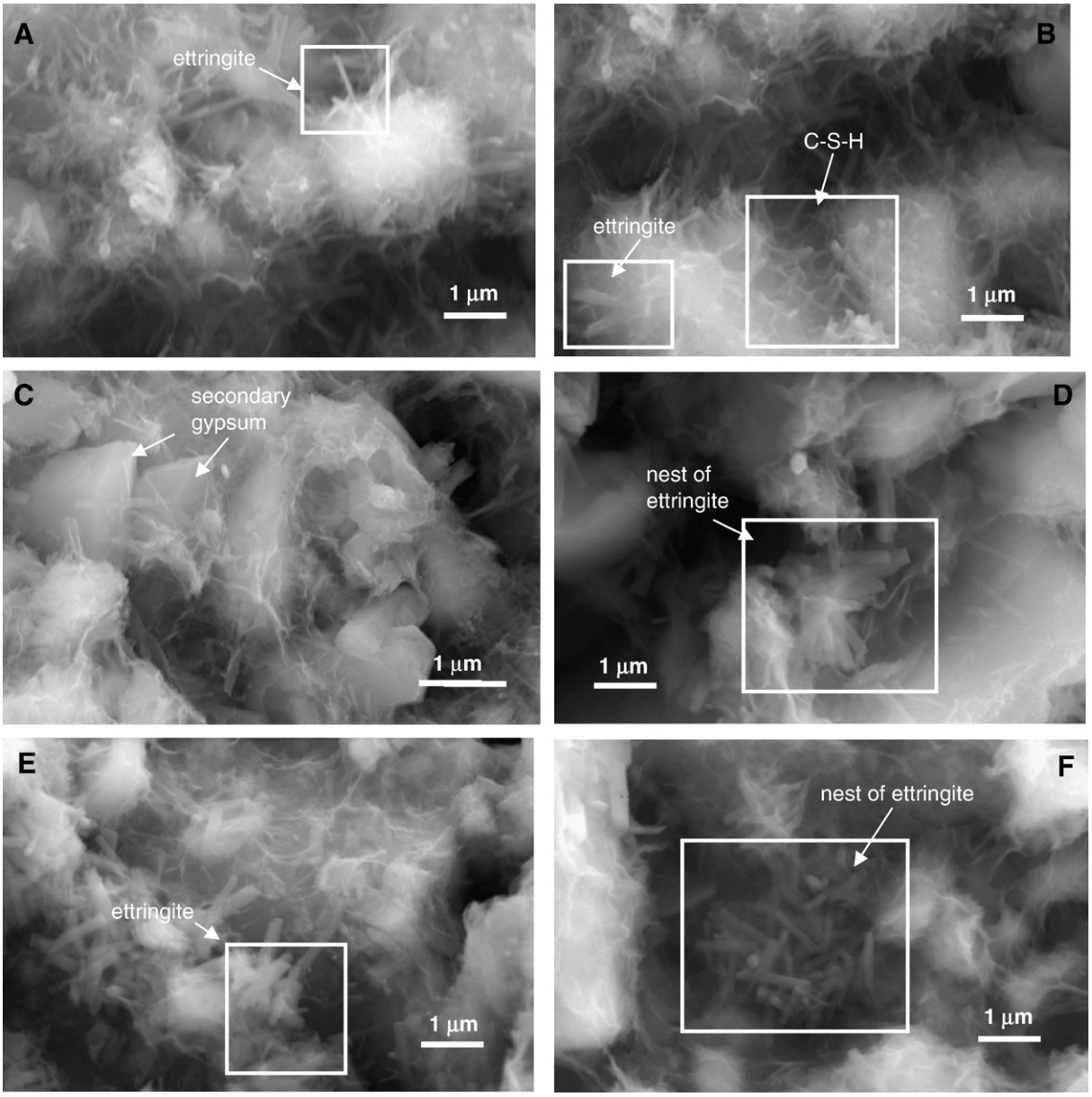


**Fig. 9.** Secondary electron images of A, B) HR-SSC, C, D) LR-SSC and E, F) LR-SSC with addition of $Al_2(SO_4)_3{\cdot}16H_2O$ and $Ca(OH)_2$ after 1 day of hydration.

surface of the particles, mainly parallel to it. The habitus of these crystals is prismatic and they generally have a length of ≤1 μm. The SE images show that less C–S–H phases are present to cover and connect the slag particles than in LR-SSC.

## 4. Discussion

### *4.1. Comparison of HR- and LR-SSC*

In both SSC systems (HR and LR) C–S–H, ettringite, gypsum and hydrotalcite are formed as hydration products. Anhydrite supplies CaO and $SO_3$ and the slag $Al_2O_3$, CaO and $SiO_2$ to form ettringite and C–S–H. In addition, hydrotalcite forms, consuming the magnesium and a part of the aluminium.

There are significant differences, however, between the two slags, in: (i) the strength development, (ii) the dissolution rate of the slag, (iii) the amount of the individual hydration products formed and also in the growth mechanisms of ettringite.

Progress of hydration may be qualitatively followed by calorimetric measurements or by the presence of $HS^-$ or Na in the pore solution from the dissolution of the slag. As sulphide is present only in the slag and as it hardly oxidizes in the closed systems investigated, $HS^-$ can be used as an indication for the rate of dissolution of the slag. Based on the total amount of sulphur present in the slag, the degree of hydration can be estimated from the comparison of the measured concentration (Fig. 6) with the calculated concentration of $HS^-$ by thermodynamic modelling (Fig. 7). The results are shown in Fig. 10. These results should be treated as qualitative estimations only as oxidation, inaccuracy of the measurements, the formation of thiosulphate, inhomogeneous dissolution of the slag and the solubility of sulphide containing solids could have an influence. These estimations give during the first days a higher dissolution rate for HR-SSC than for LR-SSC (Fig. 10) which agrees well with the observed trends in Na concentrations (Fig. 6), with the calorimetric data (Fig. 3) and the observed strength development in the SSC mortars (Table 2).

The initial dissolution rate of HR-SSC is higher than that of LR-SSC (see above) and depends on various factors. Some factors can be influenced (specific surface area, grain size distribution, and pH), whereas others (chemical and mineralogical composition of the slag) are more or less inherent properties of the respective plant that

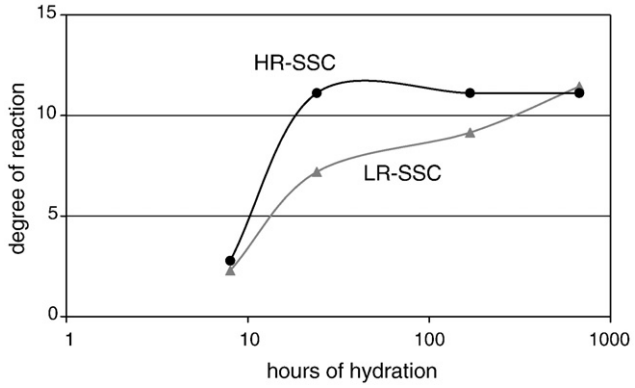


**Fig. 10.** Degree of reaction of HR- and LR-SSC after 8 h, 1, 7 and 28 days of hydration.

produces the slag. The $Al_2O_3$-concentration of both slags (Table 1) lies with 11.5 (HR-slag) and 7.7 wt.% (LR-slag) below the optimum of 13–15 wt.% [1] for SSC. HR-slag with a higher amount of $Al_2O_3$ and CaO is closer to the optimum chemical composition for slags. In addition, a lower content of $SiO_2$ increases the reactivity ($SiO_2$: 34 wt.% for HR-slag; 38 wt.% for LR-slag). LR-slag is thus initially chemically less reactive than HR-slag despite the fact that it has higher glass contents. After 28 days, however, at least a similar amount of LR-slag has reacted as of the HR-slag (Fig. 10) even though strength is still slightly lower (Table 2).

Much less ettringite is produced in LR-SSC as the system contains relative small amounts of Al. The higher amount of MgO present in LR-SSC (10.6 wt.% compared to 7.9 wt.% in HR-SSC) leads to a higher hydrotalcite formation in the LR-SSC system (see Fig. 7). Mass balance calculations using hydrotalcite $Mg_4Al_2(OH)_{14}$ indicate that in LR-SSC 2.6 g hydrotalcite per g ettringite is formed, in HR-SSC 0.32 g per g ettringite, respectively. It could be expected that hydrotalcite should be seen in XRD. However, hydrotalcite is difficult to identify in XRD for several reasons. On one hand the main reflection overlaps with the gypsum pattern, and on the other hand the detection could be complicated by the extreme compositional variability, the missing of long-range ordering which renders a rather X-ray amorphous phase [23]. If Mg is used for the formation of hydrotalcite, a high fraction of the aluminium present in LR-SSC is consumed and only little Al is available to precipitate as ettringite. In addition, LR-SSC has a much lower $Al_2O_3$ content (7.7 wt.%) than HR-SSC (11.5 wt.%). These factors together with the initial dissolution rate are responsible for the observed difference in the amount of ettringite in the hydrated SSC systems, which agrees also with the results of thermodynamic modelling as shown in Fig. 7. A comparison of the calculated volumes in HR- and LR-SSC (Fig. 11) shows that at the same degree of slag

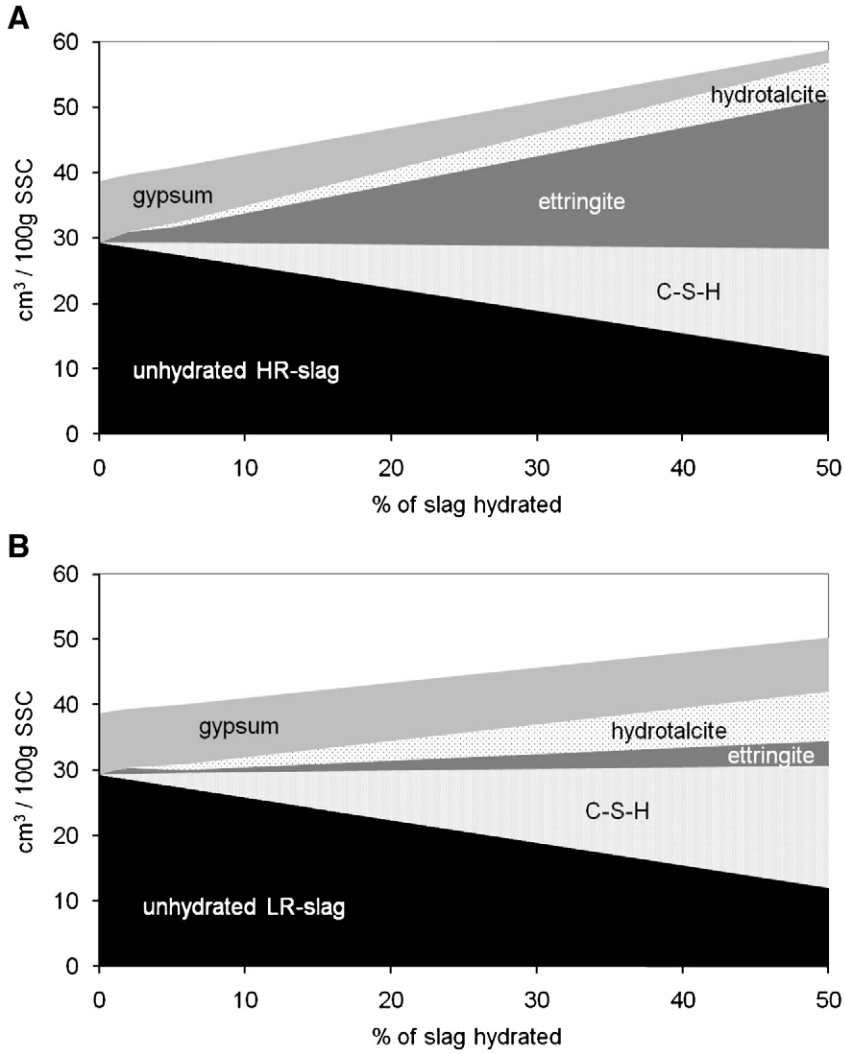


**Fig. 11.** Calculated volume percentage of the solids present in A) HR-SSC B) LR-SSC as a function of the amount of slag dissolved.

dissolution, a considerably higher volume of the solids is calculated for HR-SSC than for LR-SSC. If in both systems 50% of slag has dissolved, for HR-SSC a total volume of solids of 59 $cm^3$/ 100 g SSC is calculated which is significantly more than the volume of 50 $cm^3$/ 100 g SSC calculated for LR-SSC. Thus, the low reactivity LR-SSC does not only hydrate more slowly initially but in addition a higher degree of reaction is needed to reach the same degree of space filling. This difference in the space filling of the hydrates could be an important reason why at a similar degree of reaction as observed for LR- and HR-slag after 28 days, a somewhat higher strength is observed for the HR-slag, where more voluminous ettringite has formed.

The differing dissolution rates of the two slags could also affect growth mechanisms of the hydrates formed in HR- and LR-SSC. Stumm and Morgan [24] differ between two dissolution mechanisms at the solid–water interface: transport controlled versus surface controlled dissolution. Surface controlled dissolution results when detachment of a cationic surface group from the mineral surface via surface reaction is slow so that the concentrations adjacent to the surface build up to values essentially the same as in the surrounding bulk solution. In the case of transport controlled reactions the dissolution is relatively fast. The dissolution is limited by the rate at which dissolved products diffuse and a concentration gradient forms. In HR-SSC, where during the first day a very fast dissolution reaction is observed, transport controlled dissolution could lead to relatively high Al-concentrations near the surface resulting in increased ettringite formation right at the surface. In LR-SSC, where the slag dissolves slower, the presence of concentration gradients near the surface is less probable, leading to ettringite precipitation in the free pore space as observed experimentally.

In summary, LR-slag has a lower initial dissolution rate (Fig. 10) due to its chemical and mineralogical composition. The relatively low dissolution rate could be the reason for the preferential formation of ettringite in the empty pore space. In addition, little ettringite precipitates in LR-SSC due to the low $Al_2O_3$-content of the slag. Together with the lower volume of hydrates formed; the lower strength development compared to HR-SSC can be explained.

### *4.2. Additions to LR-SSC (LR_AC-SSC)*

In this study it was found that especially early during hydration the compressive strength of LR_AC-SSC was very low. While the addition of $Al_2(SO_4)_3{\cdot}16H_2O$ and $Ca(OH)_2$ increased the amount of ettringite formed during the first day, early compressive strength was not increased, only late compressive strength.

## 5. Conclusion

An important difference between the slag with high reactivity (HR-slag) and low reactivity (LR-slag) lies in the intrinsic dissolution rate of the slag (mainly dependent on the composition). It is found that the amount of glassy phase present in the slag is less important for the reactivity than its optimum chemical composition. In addition, in the HR-slag, which contains more $Al_2O_3$ and less MgO than the LR-slag, much more ettringite is formed and thus at the same degree of hydration the HR-slag exhibits a higher volume of the hydrates and a lower porosity. This calculated lower porosity of the HR-slag correlates with the observed higher compressive strength of the HR-slag after 28 days. The diversity in early strength development may also be attributed to the differences in the intrinsic dissolution rate of the slag which influences the mechanisms at the solid–water interface and thus the growth mechanisms of the hydrates.

Supplementary ettringite formed from the addition of $Al_2(SO_4)_3{\cdot}16H_2O$ and $Ca(OH)_2$ is observed to grow as small crystals in the pore space and is not able to interconnect the particles efficiently resulting in low initial compressive strength. It is found, that compressive strength cannot be increased just by the stoichiometric addition of constituents which are needed for the formation of a specific hydration product. A better compressive strength development of an SSC using low reactivity slag can probably only be achieved by trying to increase its intrinsic dissolution rate.

## Acknowledgments

The authors express their thanks to Holcim Group Support Ltd. for the financial support. In addition, the authors would like to thank Luigi Brunetti, Oliver Nagel, Urs Gfeller and Josef Kaufmann for their assistance in the experimental part of this study and to the reviewer for helpful comments.

## References

[1] H. Kühl, E. Schleicher, Gipsschlackenzement, Fachbuchverlag GmbH, Leipzig, 1952.
[2] H.F.W. Taylor, Cement Chemistry, 2nd edition, Thomas Telford Publishing, London, 1997.
[3] H.-G. Smolczyk, Die Hydratationsprodukte hüttensandreicher Zemente, Zem.-Kalk-Gips 5 (1965) 238–246.
[4] J. Stark, Sulfathüttenzement, Wiss. Z. Hochsch. Archit. Bauwes. Weimar 41 (6/7) (1995) 7–15.
[5] F. Keil, 2nd edition, Hochofenschlacke, vol. 7, Verlag Stahleisen M.B.H., Düsseldorf, 1963.
[6] J. Bijen, E. Niël, Supersulphated cement from blastfurnace slag and chemical gypsum available in the Netherlands and neighbouring countries, Cem. Concr. Res. 11 (3) (1981) 307–322.
[7] H.G. Midgley, K. Pettifer, The microstructure of hydrated super sulphated cement, Cem. Concr. Res. 1 (1) (1971) 101–104.
[8] D.K. Dutta, P.C. Borthakur, Activation of low lime high alumina granulated blast furnace slag by anhydrite, Cem. Concr. Res. 20 (5) (1990) 711–722.
[9] V.P. Mehrotta, A.S.A. Sai, P.C. Kapur, Plaster of Paris activated supersulphated slag cement, Cem. Concr. Res. 12 (4) (1982) 463–473.
[10] D. Li, X. Wu, J. Shen, Y. Wang, The influence of compound admixtures on properties of high-content slag cement, Cem. Concr. Res. 30 (1) (2000) 45–50.
[11] X. Fu, W. Hou, C. Yang, D. Li, X. Wu, Studies on Portland cement with large amount of slag, Cem. Concr. Res. 30 (4) (2000) 645–649.
[12] R.F.J. Barneyback, S. Diamond, Expression and analysis of pore fluids from hardened cement pastes and mortars, Cem. Concr. Res. 11 (2) (1981) 279–285.
[13] A. Gruskovnjak, B. Lothenbach, L. Holzer, R. Figi, F. Winnefeld, Hydration of alkali-activated slag Comparison with OPC, Adv. Cem. Res. 18 (3) (2006) 119–128.
[14] B. Lothenbach, F. Winnefeld, Thermodynamic modelling of the hydration of Portland cement, Cem. Concr. Res. 36 (2) (2006) 209–226.
[15] B. Lothenbach, T. Matschei, G. Möschner, F.P. Glasser, Thermodynamic modelling of the effect of temperature on the hydration and porosity of Portland cement, Cem. Concr. Res. 38 (1) (2008) 1–8.
[16] B. Lothenbach, E. Wieland, A thermodynamic approach to the hydration of sulphate-resisting Portland cement, Waste Manage. 26 (7) (2006) 706–719.
[17] D. Kulik, GEMS-PSI 2.1, PSI, Villigen, Switzerland, 2005 available at http://les.web.psi.ch/Software/GEMS-PSI/.
[18] B. Lothenbach, A. Gruskovnjak, Hydration of alkali-activated slag Thermodynamic modelling, Adv. Cem. Res. 19 (2) (2007) 81–92.
[19] S. Lamberet, Durability of ternary binders based on Portland cement, calcium aluminate cement and calcium sulphate, Thèse No 3151, Ecole polytechnique fédérale de Lausanne (2005) 83–89.
[20] K.Y. Chen, J.C. Morris, Kinetics of oxidation of aqueous sulphide by $O_2$, Environ. Sci. Technol. 6 (6) (1972) 529–536.
[21] D.J. O'Brien, F.B. Birkner, Kinetics of oxygenation of reduced sulphur species in aqueous solution, Environ. Sci. Technol. 11 (12) (1977) 1114–1120.
[22] H. Fischer, G. Schulz-Ekloff, D. Wöhrle, Oxidation of aqueous sulphide solutions by dioxygen Part I: autooxidation reaction, Chem. Eng. Technol. 20 (7) (1997) 462–468.
[23] M. Bellotto, B. Rebours, O. Clause, J. Lynch, D. Bazin, E. Elkaïm, A re-examination of hydrotalcite crystal chemistry, J. Phys. Chem. 100 (20) (1996) 8527–8534.
[24] W. Stumm, J.J. Morgan, Aquatic Chemistry, 3rd edition, John Wiley & Sons Inc., 1996.